Chemical Process Design Vol.2 No.1 (2023) 43-58

University of Sistan and Baluchestan

Chemical Process Design

Available online at http://cpd.usb.ac.ir/



Mathematical Modeling Methods and Their Application in the System Analysis for Methanol Steam Reforming Process

Mohammad Javad Peymanfard*, Alireza Sedaghat

Department of Chemical and Petroleum Engineering, Sharif University of Technology, Tehran, Iran

ARTICLE INFO

Article history:
Received: 2023-02-25
Received in revised form: 2023-08-19
Accepted: 2023-08-20
Published online: 2023-08-20

Keywords:
Methanol steam reforming; Mathematical modeling; Hydrogen production; Membrane reactors; Conservation of mass and energy; System analysis

DOI: *10.22111/CPD.2023.44973.1017*

ABSTRACT

Hydrogen is the key to achieving sustainable and clean energy in the world's future, and research in the field of optimal hydrogen production has been growing in the past years. This research discusses the mathematical modeling of the Methanol Steam Reforming Process in membrane reactors to produce hydrogen. Modeling is developed with the principles of energy, mass, and momentum conservation; In cases where the temperature is constant, only the conservation of mass will be used, and both energy and mass equations will be used in non-isothermal cases. This modeling is finally upgraded from one-dimensional to two-dimensional in the length and radial of the reactor. In each mathematical model, molecular and thermal diffusion relations are used as auxiliary equations to complete the modeling. In the final step, the effect of different variables such as temperature, pressure, and the reactor and membrane's physical conditions is analyzed to determine the optimal operating conditions for the developed mathematical models. The predictability of chemical processes behavior like the methanol steam reforming process can be achieved through basic mathematical modeling concepts. The results from the conceptual examination of the mathematical model are compared with various simulation results carried out in other articles, revealing their consistency. Basic mathematical models are superior to complex simulations as they can be leveraged to develop intelligent expert systems or predictive maintenance programs that deliver desired outcomes rapidly and cost-effectively.

1. Introduction

The increasing need for energy over time made traditional methods, such as using animals, water pressure, and even steam power, unable to provide the energy needed by the world. Because of this, the consumption of fossil fuels and coal increased tremendously, and predictions indicate that by 2050, the quantity of world energy consumption will double in contrast to today [1].

Corresponding author. Tel.: +98 (937) 9039094.
E-mail address: peymanfard.mj@gmail.com (M.J. Peymanfard)

One of the most critical problems of fossil fuels is the creation of environmental pollution due to the combustion of these fuels, which causes the production of gases such as CO_2, SO_2, and NO_2. Today, research in the field of energy has accelerated toward finding a solution to achieve sustainable and clean energy, and hydrogen seems to be the key option for the future of the world's energy. An environmentally friendly technology is fuel cells to produce electrical power. Especially, a suitable power generation device for small-scale applications is polymer electrolyte membrane fuel cells (PEMFC) [2-4]. One of the essential energy production methods is using hydrogen as a fuel in fuel cells. Also, hydrogen has many uses in the iron industry, spacecraft fuel, chemical fertilizer, and glass production. Hydrogen gas produces energy by burning with air. Since no polluting compounds such as carbon, sulfur, and nitrogen are in the structure of hydrogen gas, no harmful pollutants are produced for the environment. The only product of burning hydrogen is water, according to the following reaction:

$$H_2 + O_2 \longrightarrow 2H_2O \qquad \Delta H = 283.6\ kJ/mole \tag{1}$$

Several methods are used to produce hydrogen, including water electrolysis, coal evaporation, methanol reforming, and methane reforming. The effectiveness of these methods is evaluated according to criteria such as the geographical location of the production unit, the price of buying feed and selling products, utility services cost, and the production rate. Methods based on hydrocarbon reforming will be cost-effective if they are close to oil and gas sources; however, due to the need for advanced equipment and high technical knowledge for reforming-based processes, detailed feasibility studies should be done regarding the construction of a hydrogen production unit. In countries where electricity is affordable, the electrolysis method can also be economical in some cases.

Attention to the molecular structure of different compounds for reforming operations can also lead to identifying and comparing their general operating conditions. Methanol steam reforming can be done at low temperatures, between 200-300°C, because of having only one carbon atom and the absence of a strong carbon-carbon bond, while ethanol is reformed at a temperature of about 400°C [5, 6], and methane is reformed at a temperature higher than 500°C [7]. One of the advantages of methanol is its liquidity in atmospheric operating conditions and its biodegradability. However, the process's safety tips should be implemented strictly because methanol is very toxic and can be mixed with water easily [6, 8-10].

Generally, methanol and methane reforming are the most basic methods of hydrogen production, and other complex methods are obtained from the combination of these two methods. In Table 1, hydrogen production methods based on reforming are compared. After realizing the importance of reforming processes in the field of clean energy, and especially the superiority of the methanol steam reforming process, we continue to build mathematical models expressing this process. By examining the kinetic model of the reaction, in three chapters, we will deal with the mathematical modeling of this process with the description of its differential elements and auxiliary mathematical equations in the transfer of mass, energy and momentum. In each chapter, by changing the simplifying assumptions, we will improve the mathematical models and achieve more complex models.

2. Methanol steam reforming

Studies on the methanol steam reforming process show that the following three reactions occur in the membrane reforming reactor [12].

Methanol Steam Reforming (MSR): $$CH_3OH + H_2O \leftrightarrow 3H_2 + CO_2 \tag{2}$$

Methanol Decomposition (MD): $CH_3OH \leftrightarrow 2H_2 + CO$ (3)

Water gas shift (WGS): $CO + H_2O \leftrightarrow +CO_2 + H_2$ (4)

The production of other side products, such as CO, CO_2, and H_2O, can decrease the hydrogen gas purity in the outflow stream. However, studies have still shown that a high hydrogen purity can be achieved in the output produced during the methanol reforming process.

Table 1. Comparison of reforming methods for hydrogen production [11]

Situation	Scale	Investment	Steam Consumption	O_2 Consumption	Methane Conversion%	Pressure (bar)	Temperature (°C)	Method
Commercial	Large	100 (Ref)	High	-	65 – 95	20 – 30	800 – 900	MSR
Commercial	Small to Large	80 – 110	Optimal	High	95 – 100	30 – 85	1000 – 1450	POX
Semi Commercial	Small to Large	55 – 80	Optimal	High	95 – 100	15 – 40	800 – 1000	CPO
Commercial	Medium	70 – 90	Optimal	-	60 – 90	10	900 – 1000	CO_2 (Dry)
Commercial	Large	65 – 80	Low	High	95 – 100	20 – 70	850 – 1300	ATR
Commercial	Large	75 – 115	Medium	Low	95 – 100	20 - 30	Primary 800 Secondary 1000-1200	Combined
Semi Commercial	Large	65 – 90	Medium	Medium	95 – 100	20 - 30	Primary 800 Secondary 1000	KRES
Commercial	Medium to Large	60 – 80	Medium	Medium	95 – 100	20 - 30	Primary 450 Secondary 1000	GHR

MSR: Methanol Steam Reforming, POX: Partial Oxidation, CPO: Catalytic Partial Oxidation, ATR: Auto thermal Reforming, KRES: Kellogg Reforming Exchanger System, GHR: Gas Heated Reformer

A membrane is usually used around the reactor, so the produced products go out of the reaction section, and the process efficiency increases as the output of the products. Depending on the type of membrane, limited substances can pass through it. If needed, the flow of sweet gas also flows around the membrane to transport the products to the desired location. The research results indicate that even a small amount of CO reduces the efficiency of the reaction due to entering into the reaction related to the competition of absorption with hydrogen on the membrane surface. Hence, the hydrogen production increases when the WGS reaction progresses better [13].

On the other hand, connected reactors are used through a membrane to decrease the CO_2 production, a harmful compound to the environment. Feed and incoming streams are preheated before entering the reactor and release heat during the reaction; therefore, reactor membranes should be compatible with these thermal loads.

The MSR process can be evaluated using different criteria. [14], by examining the reactions mentioned earlier by a palladium membrane, showed that the reaction's efficiency decreases with the increase in the catalyst particles size. Ghasemzadeh et al. [15] investigated the design of different reactors to find a suitable reactor for a methanol reforming reaction. Their research included three types of silica membrane reactor, palladium membrane, and conventional reactor, and showed that the efficiency of conventional reactors is less than membrane reactors. Also, in their research, it was shown that at low temperatures and high pressure, methanol conversion in palladium membrane is more than in silica.

2.1. Kinetic modeling

Various kinetic models have been studied and developed to describe the methanol reforming process; the most famous kinetic model is based on the Langmuir-Hinshelwood equations on the $Cu/ZnO/Al_2O_3$ catalyst. Pepli et al. [16] have presented the reaction rate expressions of triple reactions inside the reactor by Equations (5–7).

$$r_{MSR} = \frac{K_{MSR}K_1\left(p_{t_{CH_3OH}} - \left(p^3{}_{t_{H_2}} p_{t_{CO_2}}\right)\right)C_1 2C_{S1}C_g}{\left(p^{0.5}{}_{t_{H_2}} + K_1 p_{t_{CH_3OH}} + K_2 p_{t_{CO_2}} p_{t_{H_2}} + K_3 p_{t_{H_2O}}\right)\left(1 + K_4^{0.5} p^{0.5}{}_{t_{H_2}}\right)} \quad (5)$$

$$r_{MD} = \frac{K_{MD}K_5\left(p_{t_{CH_3OH}} - \left(\frac{p_{t_{H_2}}{}^2 p_{t_{CO_2}}}{K_{MD,T}}\right)\right)C_2 2C_{S2}C_g}{\left(p_{t_{H_2}}{}^{0.5} + K_5 p_{t_{CH_3OH}} + K_6 p_{t_{H_2O}}\right)\left(1 + K_7{}^{0.5} p_{t_{H_2}}{}^{0.5}\right)} \quad (6)$$

$$r_{WGS} = \frac{K_{WGS}K_1 p_{t_{H_2}}{}^{0.5}\left(p_{t_{CO}} p_{t_{H_2O}} - \left(\frac{p_{t_{H_2}} p_{t_{CO_2}}}{K_{WGS,T}}\right)\right)C_g C_1^2}{\left(p_{t_{H_2}}{}^{0.5} + K_1 p_{t_{CH_3OH}} + K_2 p_{t_{CO_2}} p_{t_{H_2}} + K_3 p_{t_{H_2O}}\right)^2} \quad (7)$$

In the reaction rate relations (5-7), the components partial pressure values are evaluated from Dalton's partial pressure law.

$$P_i = P\frac{F_i}{\sum F_i} \quad (8)$$

F_i is the component's molar flow rate present in the gas flows inside the reactor; P_i is the component's partial pressure, and the total pressure of the flow is denoted by P. The kinetic constants of reaction rate equations according to the Arrhenius equation, are presented as follows [17]:

$$K_i = K_{0_i} \times \exp\left(\frac{-E_i}{RT}\right) \quad (9)$$

E_i is the reaction activation energy, and K_{0i} is the pre-exponential coefficient.

Table 2. MSR process kinetic parameters [17]

K_i	K_{0i} (m^2/s. mole)	E_i (kj/mole)
K_{MSR}	7.4×10^{14}	102800
K_{MD}	3.8×10^{20}	170000
K_{WGS}	5.9×10^{13}	876000
K_1	6.55×10^{-3}	20000
K_2	2.3×10^{9}	100000
K_3	4.74×10^{-3}	20000
K_4	5.43×10^{-6}	-50000
K_5	36.9	-20000
K_6	36.9	-20000
K_7	3.86×10^{-3}	-50000

The concentration constants in the reaction rate equations and partial rate expressions that are not based on the Arrhenius equation are as follows [17].

$$C_1 = C_2 = 7.5\times10^{-6} \quad (10)$$

$$C_{S1} = C_{S2} = 1.5\times10^{-5} \quad (11)$$

$$C_g = 1.02\times10^{-5} \quad (12)$$

$$K_{MSR_T} = \exp\left[-\frac{4421.82}{T} + 3.57\ln(T) + \left(8.99\times10^{-3}\times T\right) - \left(8.22\times10^{-6}\times T^2\right) + \left(3.35\times10^{-9}\times T^3\right) - \left(5.41\times10^{-13}\times T^4\right) - 6.13\right] \quad (13)$$

$$K_{MD_T} = \exp\left[-\frac{9305.38}{T} + 4.85\ln(T) + \left(4.33\times10^{-3}\times T\right) - \left(6.01\times10^{-6}\times T^2\right) + \left(2.69\times10^{-9}\times T^3\right) - \left(4.51\times10^{-13}\times T^4\right) - 7.39\right] \quad (14)$$

$$K_{WGS_T} = \exp\left[-\frac{4883.56}{T} + 1.28\ln(T) + \left(4.66\times10^{-3}\times T\right) - \left(2.21\times10^{-6}\times T^2\right) + \left(6.61\times10^{-10}\times T^3\right) - \left(9\times10^{-14}\times T^4\right) + 1.26\right] \quad (15)$$

3. Mathematical modeling of isothermal single-shell reactor

The model complexity depends on the assumptions that determine its degree of simplicity. This model is the simplest compared to the three models that have been studied. A view of a single-shell membrane reactor is shown in Fig. 1. These reactors are in the form of two tubular sections with a membrane between them that does not join into the reactions. The input feed to this reactor mainly includes methanol and water vapor, which enters the central tube called the reaction zone that filled with a bed of catalysts. The outer part around the reaction zone is the permeated zone of the reactor, which, in addition to transferring the hydrogen separated by the sweep gas, causes it to leave the feed stream. Sweep gas, in addition to the transfer and discharge of hydrogen, creates a driving force due to the reduction of the pressure in the outer layer so that the gaseous products of the reaction in the central tube penetrate out of the membrane. In this model, the membrane used is made of palladium-silver, which is only selective for hydrogen and allows this gas to pass [18].

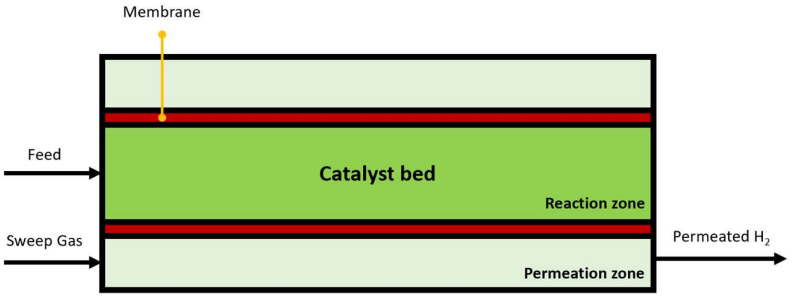


Fig. 1. Membrane single-shell steam reforming reactor

3.1. Assumptions

To solve the one-dimensional mathematical model, the following assumptions are considered:

1- The temperature gradient along the reactor, resulting from the heat transfer in this direction, can be ignored.

2- Mass penetration along the length is negligible compared to mass transfer in the form of mass flow.

3- The type of flow in both inside and outside sections is considered as Plug Flow.

4- In this model, the ratio of the catalyst bed length to the catalyst particles size is greater than 50, and the phenomenon of diffusion and penetration in the longitudinal and radial directions can be ignored.

5- Temperature and concentration changes in the radial direction have been ignored, so the modeling element is one-dimensional.

6- Due to the smallness of the catalyst grains (diameter less than 3 mm), the temperature and concentration distribution inside them is ignored.

7- Constant pressure conditions are assumed along the catalyst bed. Due to the high flow intensity of the sweeping gas in the permeation zone, we assume constant pressure in this section.

8- A heat source outside the reactor stabilizes the temperature at the desired value.

9- The resistance against mass transfer from the membrane is assumed to be negligible due to its microporous structure.

10- The process is modeled in a steady state, and we will not have any accumulation during the reactor.

3.2 Element mass balances

According to the assumptions in the previous section, a one-dimensional differential element is used along the length of the reactor (z), as shown in Fig. 2 and the mass balance for it is written as follows:

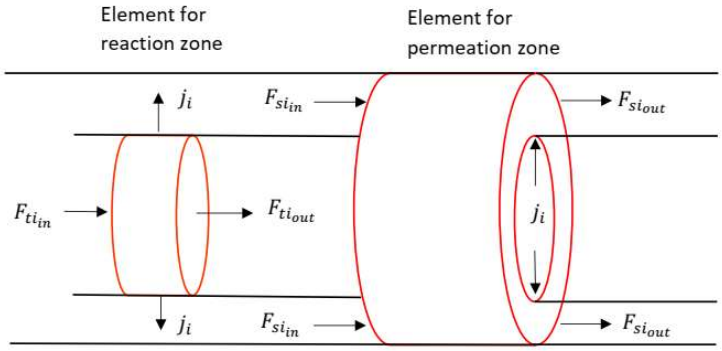


Fig. 2. The elements of reaction and permeation zone

The general conservation of mass law:

Inputs – Outputs + Generation – Consumption = Accumulation

Mass balance on the reaction zone element:

$$F_{t_{in}} - F_{t_{out}} + \pi R_1^2 dz \times \sum_{j=1}^{M} \left[\eta_j \left(\pm v_{ij} . r_j . \rho_B \right) - 2\pi R_1 dz j_i \right] = 0 \tag{16}$$

By dividing the above equation by dz, we can reach the following equation:

$$\frac{dF_{ti}}{dz} = \pi R_1^2 dz \times \sum_{j=1}^{M} \left[\eta_j \left(\pm v_{ij} . r_j . \rho_B \right) - 2\pi R_1 dz j_i \right] \tag{17}$$

Mass balance on the permeation zone element:

$$F_{s,i_{in}} - F_{s,i_{out}} - 2\pi R_2 dz j_i = 0 \xrightarrow{\div dz} \frac{dF_{s,i}}{dz} = 2\pi R_2 dz j_i \tag{18}$$

The total formation rate of each component can obtain as follows:

$$-r_i = \sum_{j=1}^{M} \eta_j \left(\pm v_{ij} r_j \right) \tag{19}$$

$$-r_{Methanol} = r_{MSR} + r_{MD} \tag{20}$$

$$-r_{Water} = r_{MSR} + r_{WGS} \tag{21}$$

$$-r_{Hydrogen} = -3r_{MSR} - 2r_{MD} - r_{WGS} \tag{22}$$

$$-r_{CarbonMonoxide} = -r_{MD} + r_{WGS} \tag{23}$$

$$-r_{CarbonDioxide} = -r_{MSR} - r_{WGS} \tag{24}$$

One of the common membranes for hydrogen separation is palladium silver membrane. Hydrogen in these types of membranes is more permeable than other gas components in the system. The hydrogen permeation flux can be written as follows:

$$J_{H_2} = \frac{P_M}{\delta} \left(p^n{}_{H_2,tube} - p^n{}_{H_2,shell} \right) \tag{25}$$

J_{H2} is H_2 mass flux; $p_{H_2\,tube}$ is Hydrogen pressure in the tube (reaction zone), and $p_{H_2\,shell}$ is Hydrogen low pressure in the shell (permeate zone); n is assumed to be equal to 0.5 due to Sievert's half-power pressure law; δ is the membrane thickness; The permeability coefficient of hydrogen (P_M) based on the Arrhenius law, only depends on the temperature as follows.:

$$P_M = P_{M,O} \times \exp\left(\frac{-E_M}{RT}\right) \tag{26}$$

Finally, the hydrogen flux via the membrane is as follows [19-23]:

$$J_{H_2} = \beta_C \frac{P_{M,O}}{\delta} \times \exp\left(-\frac{29160}{RT}\right)\left(p^{0.5}{}_{H_2,tube} - p^{0.5}{}_{H_2,shell}\right) \tag{27}$$

According to the assumptions, the studied membrane is only permeable to hydrogen. Therefore, with two equations for the permeation zone (shell side) and five equations for the reaction zone (tube side), the reactor performance can be fully determined. The equations expressing the material flow distribution at the inside and outside zone will be as follows:

Final differential equations for reaction zone:

$$\frac{dF_{t,CH_3OH}}{dz} = \pi R_1^{\,2} \rho_B \left[-r_{MSR} - r_{MD}\right] \tag{28}$$

$$\frac{dF_{t,H_2O}}{dz} = \pi R_1^{\,2} \rho_B \left[-r_{MSR} - r_{WGS}\right] \tag{29}$$

$$\frac{dF_{t,H_2}}{dz} = \pi R_1^{\,2} \rho_B \left[3r_{MSR} + 2r_{MD} + r_{WGS}\right] - 2\pi R_1 J_{H_2} \tag{30}$$

$$\frac{dF_{t,CO}}{dz} = \pi R_1^{\,2} \rho_B \left[3r_{MD} - r_{WGS}\right] \tag{31}$$

$$\frac{dF_{t,CO_2}}{dz} = \pi R_1^{\,2} \rho_B \left[r_{MSR} + r_{WGS}\right] \tag{32}$$

Final differential equations for permeation zone:

$$\frac{dF_{s,H_2}}{dz} = 2\pi R_2 J_{H_2} \tag{33}$$

$$\frac{dF_{s,SweepGas}}{dz} = 0 \tag{34}$$

4. Non-isothermal coupled membrane reactor model

The main difference between this model and the previous one is that the exothermic reaction of methanol provides heat for the endothermic reaction of reforming inside the reactor inner membrane. The methanol combustion reaction is as follows [24]:

$$CH_3OH + \frac{3}{2}O_2 \rightarrow 2H_2O + CO_2 \qquad \Delta H_{C,298K} = -6.752\times10^5 \left(\frac{J}{mole}\right) \tag{35}$$

Chu, X., et al. [25] used catalysts based on Pt/Al_2O_3 in the methanol combustion section and presented the kinetic equation expressing the rate of methanol combustion as follows:

$$r_c = k_c \exp\left(\frac{-E_c}{RT}\right) C_{CH_3OH}^{1.4} \tag{36}$$

4.1. Assumptions

These assumptions used for the mathematical modeling of this reactor [11]:

1- There is a temperature gradient along the reactor.

2- Mass diffusion along the reactor is insignificant compared to mass transfer with the convection mechanism.

3- The reactor flow is considered a Plug Flow.

4- The ratio of the catalyst particle size to its bed length is less than 0.02, so the diffusion and penetration along the length and radius can be ignored.

5- The concentration gradient in the radial direction has been ignored, and the element is one-dimensional.

6- Due to the smallness of the catalyst particles (diameter is less than 3 mm), the temperature and concentration distribution inside them is ignored.

7- The isobar condition is considered for gas reactions along the catalyst bed, and constant pressure is assumed due to the high flow intensity of the sweeping gas in the shell part.

8- The resistance against mass transfer from the membrane is assumed to be insignificant due to its microporous structure.

9- The process is modeled in a steady state, and we will not have any accumulation during the reactor.

4.2. Mass balance

The differential equations of mass changes in the penetration and the reforming membranes do not differ from the previous model due to the same assumptions. Hence, it is only enough to derive the mass equations of the combustion side. Because only one reaction takes place on the combustion side and there is no membrane in the shell of it, the only factor that decreases or increases the flow rate is the methanol combustion reaction. According to the assumptions, the one-dimensional cylindrical shell's differential element along the reactor length (z) is used. Therefore, the equations are derived for every four components in the combustion reaction.

$$\frac{dF_{CH_3OH}}{dz} = -r_c A_c \tag{37}$$

$$\frac{dF_{H_2O}}{dz} = 2r_c A_c \tag{38}$$

$$\frac{dF_{O2}}{dz} = -1.5r_c A_c \tag{39}$$

$$\frac{dF_{CO_2}}{dz} = -r_c A_c \tag{40}$$

where, $A_c = 2\pi\ (R_c^2 - R_r^2)$ is the surface of the fluid passing through the cylindrical combustion side; R_r is the outer radius of the reforming reaction side; R_c is the outer radius of the methanol combustion membrane (Fig. 3); r_c is the kinetic equation expressing the rate of methanol combustion.

4.3. Energy balance

Methanol reforming reaction is endothermic, and using thermal furnaces and utility is the easiest way to provide this heat. This condition, which is the isothermal, steady-state, and one-dimensional model, was examined in the previous section. In this case, the reaction temperature does not remain constant due to the use of the exothermic reaction of

methanol combustion. As a result, to describe the temperature gradient along the reactor, it is required to apply the energy balance and derive the temperature equation.

Different thermal energies can enter the system, consume, produce or leave the reactor in the following ways:

1) The energy of input and output streams to the reactor

2) Energy caused by reactions inside the reactor

3) Input energy through the furnace

The energy of input and output streams is as below:

$$q_i = F_i C_{pi}\left(T - T_{ref}\right) \tag{41}$$

Enthalpy of reactions is as follows:

$$\Delta_r H_i(T) = \Delta_r H^0_{298K} + \sum v_{ij} \times \int_{298K}^{T} C_{pi}(T)\,dT \tag{42}$$

$$C_{pi}(T) = A_j + B_j T \times 10^{-3} + C_j T^2 \times 10^{-6} + \frac{D_j}{T^2} \times 10^5 \tag{43}$$

The energy balance is written for the three main differential elements of the reactor (central, reforming, and combustion sides) according to Fig. 3 to derive the temperature equations for each wall.

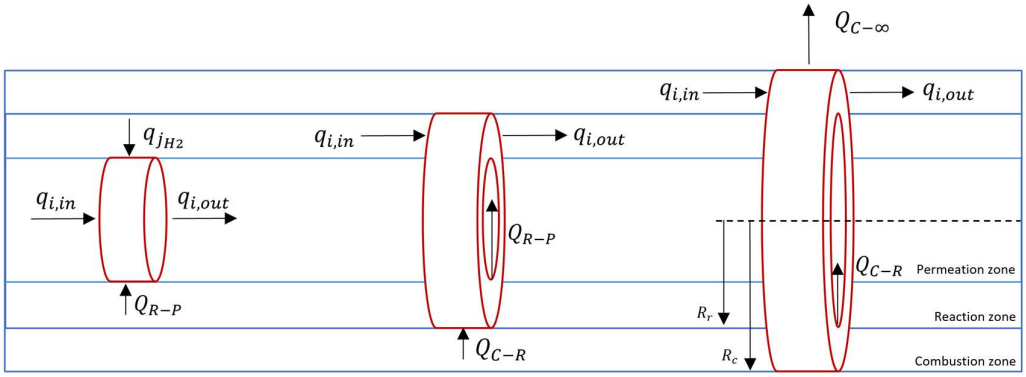


Fig. 3. Differential elements, input, and output energy flows to the penetration, reaction, and combustion sides

The general conservation of energy law:

Inputs – Outputs + Generation – Consumption = Accumulation

(a): Energy balance on the penetration section (central side):

$$\sum F_{i_{in}} C_{P,i_{in}} dT_P + U_{R-P}\left(2\pi R_m dz\right)\left(T_R - T_P\right) + \left(2\pi R_m dz\right) J_{H_2} C_{P,H_2} - \sum F_{i_{out}} C_{P,i_{out}} dT_P = 0 \tag{44}$$

By dividing the above equation by *dx*, we can reach the following equation:

$$\sum F_{i_{out}} C_{P,i_{out}} \frac{dT_P}{dz} - \sum F_{i_{in}} C_{P,i_{in}} \frac{dT_P}{dz} = U_{R-P}\left(2\pi R_m\right)\left(T_R - T_P\right) + 2\pi R_m J_{H_2} C_{P,H_2} \tag{45}$$

(b): Energy balance on the reformer section:

$$\sum F_{i_{in}} C_{P,i_{in}} dT_R + \sum\left(-r_i\right)\Delta H_j A_r dz + U_{R-C}\left(2\pi R_C dz\right)\left(T_C - T_R\right) - U_{R-P}\left(2\pi R_P dz\right)\left(T_R - T_P\right) - \sum F_{i_{out}} C_{P,i_{out}} dT_R = 0 \tag{46}$$

By dividing the above equation by *dx*, we can reach the following equation:

$$\sum F_{i_{out}} C_{P,i_{out}} \frac{dT_R}{dz} - \sum F_{i_{in}} C_{P,i_{in}} \frac{dT_R}{dz} = \sum\left(-r_i\right)\Delta H_j A_r + U_{R-C}\left(2\pi R_C\right)\left(T_C - T_R\right) - U_{R-P}\left(2\pi R_P\right)\left(T_R - T_P\right) \tag{47}$$

(c): Energy balance on the combustion section:

$$\sum F_{i_{in}} C_{P,i_{in}} dT_C + \sum (-r_i) \Delta H_j A_C dz - U_{R-C} (2\pi R_C dz)(T_C - T_R) - U_{R-\infty} (2\pi R_C dz)(T_R - T_\infty) - \sum F_{i_{out}} C_{P,i_{out}} dT_C = 0 \quad (48)$$

By dividing the above equation by *dx*, we can reach the following equation:

$$\sum F_{i_{out}} C_{P,i_{out}} \frac{dT_C}{dz} - \sum F_{i_{in}} C_{P,i_{in}} \frac{dT_C}{dz} = \sum (-r_i) \Delta H_j A_C - U_{R-C} (2\pi R_C)(T_C - T_R) - U_{C-\infty} (2\pi R_C)(T_C - T_\infty) \quad (49)$$

where $A_c = 2\pi (R_c^2 - R_r^2)$ and $A_r = 2\pi (R_r^2 - R_p^2)$ are the surface of each element. To calculate the variable *J*, several equations have been presented in general form of equation (27).

5. Two-dimensional non-isothermal single-membrane reactor model

For this case, the stream is not assumed to be a plug flow. Hence, the momentum balance describes the fluid movement inside the reactor.

5.1. Assumptions

These assumptions are applied for modeling of this reactor:

1- Transfer of heat, mass, and momentum is in *r* and *z* dimensions.

2- Steady-state conditions

3- Reactor operation and reaction are assumed to be quasi-steady-state.

4- The temperature varies throughout the reactor length.

5- The dispersion and penetration of the catalyst into the fluid are negligible.

6- A heat source outside the reactor provides heat for the reforming reaction.

7- Resistance to mass transfer in the membrane is negligible.

5.2. Momentum balance

Due to the catalyst bed and fluid flow with a low Reynolds number inside the reactor, the Darcy–Brinkman equation are used to model the fluid flow [26, 27].

$$\frac{\mu}{k} \underline{U} = \nabla . \left[-p + \frac{1}{\varepsilon_{bed}} \left\{ \mu \left(\nabla \underline{U} + (\nabla \underline{U})^T \right) - \frac{2}{3} \mu (\nabla . \underline{U}) \right\} \right] \quad (50)$$

$$\nabla . (\rho \underline{U}) = 0 \quad (51)$$

$$\rho = \frac{p}{RT} \sum_{i}^{Components} x_i M_i \quad (52)$$

Also, the present components in the system are H_2, CO_2, CO, CH_3OH, and H_2O, where the velocity field is $\underline{U}$ and the permeability of the catalyst bed is *k*.

5.3. Mass balance

For mass conservation, Stephen Maxwell's law is applied [26, 28]:

$$\nabla . \left(\rho \omega_i \underline{U} - \rho \omega_i \sum\nolimits_i \bar{D}_{ij} \left(\nabla x_j + (x_j - \omega_i) \frac{\nabla p}{p} \right) \right) = \sum_{j=1}^{M} \pm v_{ij} r_j \quad (53)$$

where *i* and *j* mean the reaction compounds, H_2, CO, CO_2, H_2O, CH_3OH, and *k* is the reaction counter. Also, ω_i is the mass fraction of the components; x_j is the molar fraction of components, and $\overline{D}_{ij}$ is the diffusion coefficient.

5.4. Energy balance on the catalyst bed

Here three types of heat transfer, conduction, convection, and heat of reaction, are considered.

The general conservation of energy law at steady-state:

Inputs – Outputs + Generation – Consumption = Accumulation = 0

$$2\pi rdrdz\left(q_{in}-q_{out}\right)+\sum_{j=1}^{M}\Delta H_j r_j=\rho \underline{U} AC_P T \tag{54}$$

By dividing the above equation by 2π*dzdr*, we can reach the following equation:

$$\nabla.\left(-k_{eff}\nabla T\right)+\rho C_P \underline{U}.\nabla T=\sum_{j=1}^{M}\Delta H_j r_j \tag{55}$$

where R_k is the reaction rate of k_{th} and k_{eff} is the effective coefficient of conductive heat transfer of the catalytic bed.

5.5. Energy balance on the reactor membrane

The only heat transfer mechanism in this section is conduction.

$$2\pi rdrdz\left(q_{in}-q_{out}\right)=0 \tag{56}$$

By dividing the above equation by 2π*dzdr*, we can reach the following equation:

$$k_{ss}\nabla^2 T_2=0 \tag{57}$$

where k_{ss} is the conductive heat transfer coefficient of stainless steel which is the material of reactor body.

5.6. Trans-membrane H_2 flux

The H_2 flux across the Pd–Ag membrane under reaction conditions is given by the below equation [26]:

$$J_{H_2}=\left(\theta_H+\theta_V\right)q_0\exp\left(\frac{-E_H}{RT}\right)\left(p^{0.5}{}_{H_2,ret}-p^{0.5}{}_{H_2,perm}\right) \tag{58}$$

where

$$\left(\theta_H+\theta_V\right)=\frac{1+\sqrt{K_H p_{H_2}}}{1+\sqrt{K_H p_{H_2}}+\left(K_{H_2O}p_{H_2O}\right)+\sqrt[3]{K_{CO}p_{CO}}+\sqrt{K_{CO_2}p_{CO_2}}+\sqrt{K_{CH_3OH}p_{CH_3OH}}+\frac{K_1\left(K_{CH_3OH}p_{CH_3OH}\right)}{\sqrt{K_H p_{H_2}}}+\frac{K_1K_2\left(K_{CH_3OH}p_{CH_3OH}\right)}{K_H p_{E_2}}} \tag{59}$$

The above constants are calculated in [12]. Also, θ_V and θ_H are the ratio of the bare surface to the membrane surface and the ratio of the membrane surface that is covered with hydrogen, respectively.

5.7. Effective radial diffusivities

The effective radial diffusivities according to Gunn are as below [26, 29]:

$$\frac{1}{Pe_{ij,eff}}=\frac{ud_{particle}}{D_{ij,eff}}=\frac{1}{Pe_f}+\frac{\varepsilon_{bed}}{\tau\,\mathrm{Re}\,Sc_{ij}} \tag{60}$$

$$Pe_f=40-29\exp\left(\frac{-7}{\mathrm{Re}}\right) \tag{61}$$

where $d_{particle}$ is the catalyst particles radius, ε_{bed} is the porosity of catalyst bed, and the τ is tortuosity.

5.8. Effective bed thermal conductivity

The effective bed thermal conductivity using the below equation is as follows [26, 30]:

$$\frac{K_{eff}}{K_{fluid}} = K_{cond} + K_{conv} \tag{62}$$

$$K_{cond} = \varepsilon_{bed} + \frac{1-\varepsilon_{bed}}{0.22\varepsilon^{2}_{bed} + \frac{2}{3}\left(\frac{K_{fluid}}{K_{solid}}\right)} \tag{63}$$

$$K_{conv} = \frac{\mathrm{Re}\times \mathrm{Pr}}{8.65\left(1+19.4\left(\frac{d_{particle}}{2R_{iw}}\right)^{2}\right)} \tag{64}$$

where R_{iw} is the inner radius of reactor.

5.9. Effective wall to bed heat transfer coefficient

The effective wall to bed heat transfer coefficient using the below equation is as follows [26, 30]:

$$h_{eff} = h_{conduction} + h_{convection} \tag{65}$$

$$h_{conduction} = \left(2\varepsilon_{particle} + \frac{1-\varepsilon_{particle}}{\frac{k_{fluid}}{3k_{solid}} + 0.0024\frac{2R_{iw}}{d_{particle}}}\right)\left(\frac{k_{fluid}}{d_{particle}}\right) \tag{66}$$

$$h_{convection} = 0.0835\times \mathrm{Re}^{0.53}\,\mathrm{Pr}^{0.33}\,\frac{k_{fluid}}{d_{particle}} \tag{67}$$

6. Results and discussion

In this section, changing different factors, such as temperature, membrane thickness, the ratio of input materials, and reactor length, will be discussed to find the optimal operating conditions for the MSR process, and the results of solving each mathematical model will be compared.

6.1. Isothermal single-shell reactor

Because the equilibrium reaction of MSR is endothermic, the conversion increases with the rise in the overall reactor temperature. Also, by increasing the amount of methanol input compared to steam, the conversion percentage will not change much due to the balance of the reforming reactions. To the center of the reactor, the amount of H_2 inside the central tube, which is the reforming part of this model, is increasing; Because in the initial parts of the reactor, the reaction rate and H_2 production is higher than the penetration rate and exit of H_2 from the membrane; But in the second half, due to the decrease in the rate of reaction, the H_2 concentration inside the central tube gradually decreases, which will also decrease the rate and gradient of hydrogen penetration. Also, if a membrane is selected that is only selective for hydrogen, the concentration of CO and CO_2 will have a downward trend during the reactor because they cannot pass through the membrane.

By keeping the temperature constant and decreasing the ratio of methanol to steam input in two stages, Qureshi, F., et al. has shown that by decreasing the ratio of methanol to steam input in the feed of the reforming reaction zone,

the amount of hydrogen penetrated the shell decreased and the concentration of hydrogen in the central tube region increased slightly [31]. Also, by increasing this ratio, the discharge of carbon dioxide increases, and the carbon monoxide flow decreases.

6.2. Non-isothermal coupled membrane reactor model

The most important difference between this model and the previous one is the temperature gradient in each wall. As mentioned, the MSR reaction is endothermic and along the reactor, temperature reduces. At first, because of the methanol combustion reaction and heat release in the reactor's initial parts, its temperature increases. However, finally, the temperature of the combustion section decreases; because the heat of this part is transferred to the reforming section to provide heat for the reforming reactions. The central tube temperature or the penetration section increases slowly due to the heat of the reforming wall.

Across the reactor, the H_2 recovery increases, which is the primary goal of a reforming membrane reactor. However, at the end of the reactor, reducing the amount of methanol remaining for reforming and increasing the H_2 concentration in the permeation zone has caused a decrease in the driving force for the transfer and permeation of H_2 from the membrane. The H_2 recovery process slows down, which is also true for the isothermal model.

Because of the endothermic MSR reaction, the final fractional conversion of methanol increases by a temperature increase in the reactor. Another method to increase the fractional conversion of methanol is to reduce the thickness of the membrane. The smaller the membrane thickness, the greater the H_2 penetration. Therefore, the methanol reforming equilibrium reaction will move towards producing more hydrogen, and the percentage of methanol conversion will increase. Therefore, new research on the membrane structure of the reforming process is recommended.

Talaghat and Naamaki [11] have researched the reuse of methanol exiting from the end of the reforming wall as input feed to the combustion section. According to the previous section, the fractional conversion increases along the reactor. However, the final fractional conversion is lower than the state in which fresh methanol is used as the combustion zone feed.

For this model, the temperature of the three reactor zones changes. At the end of the reactor, the outlet flow temperature of the reforming zone equals the input flow to the combustion section, which is considered a boundary condition for solving the equations. Either in the case of fresh methanol feed or the case of methanol feed from the output of the reforming section, the hydrogen recovery is approximately the same, or the new method of using unreacted methanol does not lead to higher efficiency in hydrogen recovery.

6.3. Two-dimensional non-isothermal single-membrane reactor model

According to the modeling results, hydrogen production and permeation rise with the pressure and temperature gradient increase between the shell and the membrane. At high pressure, temperature, and residence time, all reactors (with and without membrane) will have the same methanol fractional conversion, and almost all methanol is consumed. Hydrogen separation in membrane reactors can increase this fraction. However, the fraction is limited because of hydrogen adsorption in the catalyst's pores and trapping in the membrane's pores. It means only a limited amount of hydrogen can be extracted.

Dimensions of the reactor based on the residence time should be adjusted so that after the 100% conversion of methanol, products are removed from the reactor. An increase in the residence time causes more possibilities for the penetration of other reaction products inside the membrane and a decrease in hydrogen purity. Adsorption of carbon monoxide is the biggest obstacle to reducing hydrogen flux. Because it is the smallest molecule in the reactor after hydrogen. On the other hand, at a high rate and short residence time, methanol conversion is low and is the most important factor preventing the penetration of hydrogen, methanol, and water.

Pure palladium alloys can prevent CO adsorption and increase hydrogen production by up to 40moles/(m^3s). This number is obtained from the calculated value in the simulation and is different from the actual conditions. In CO adsorption, the higher the ratio of water to methanol in the feed, the lower the amount of CO adsorbed by the membrane. However, a higher ratio of water to methanol can reduce hydrogen production because with one mole of input steam, one mole of hydrogen is produced in the water shift gas reaction, and 2 moles of hydrogen are obtained in the methanol decomposition reaction [26].

The reactions kinetics and the quantity of methanol consumption can examine with the ratio of CO to CO_2. Due to the separation of H_2 in membrane reactors and the balance of the WGS reaction, the quantity of CO_2 is higher than CO. However, experiments show that this ratio increases in both membrane reactors by decreasing the residence time at first. This ratio in typical (membrane-free) reactors decreases with a constant slope. The methanol consumption of the MSR reaction is more than that of the methanol decomposition reaction [26].

7. Conclusion

This paper developed three mathematical models of H_2 production using the MSR process. Each model's simulation results and operational parameters' effect on the process performance were examined. According to the modeling results, the conversion of methanol in packed bed membrane reactors is about 5-10% higher than the packed bed reactors. The adsorption of species other than hydrogen in the system to the membrane decreases the H_2 transfer flux from the membrane and reduces hydrogen production. Therefore, one of the important fields of research on reforming reactors is the research and development of membranes resistant to the adsorption of substances such as CO. In membrane reactors, because of the CO production in the reforming reaction and its consumption in the WGS reaction, the concentration of CO first increases and then decreases. Hydrogen is produced in the reforming reaction and exits the reaction zone through the membrane. Permeation of H_2 outside the reaction zone shifts the equilibrium towards product formation. At the beginning of the reactor, due to the high methanol concentration, the rate of H_2 production is higher than the exit rate from the membrane. Hence, the H_2 concentration increases, but at the end of the reactor, the concentration of hydrogen decreases. In order to reduce the partial pressure of the permeation zone, sweep gas with a high flowrate is used. On the other hand, increasing the reaction zone pressure causes more H_2 to pass along the membrane because of increases in the penetration driving force. Based on the equilibrium in the MSR reaction, due to the presence of more moles of gas produced on the reaction right side than gas moles consumed on the reaction left side, reducing the pressure leads to further progress of the reaction. Due to the endothermicity of the reaction, an increase in the temperature of the reaction zone also leads to further progress.

Nomenclature

Symbols

θ_V	Fraction of vacant sites on membrane surface

F_i	Molar flow rate of ith component (mol s^{-1})
P_i	Partial pressure of ith component (bar)
P	Total pressure of the flow (bar)
E_i	Reaction activation energy (kj mol^{-1})
k_{0i}	Pre coefficient of reaction rate (m^2 s^{-1} mol^{-1})
J_i	Molar flux of ith component (mol m^{-2} s^{-1})
r_j	Rate of jth reaction (mol kg^{-1} s^{-1})
Ac	Surface of the fluid passing through the cylindrical combustion side (m^2)
Rr	Outer radius of the reforming reaction side (m)
Rc	Outer radius of the methanol combustion membrane (m)
$\Delta_r H_i$	Reactions enthalpy (kJ mol^{-1})
$d_{particle}$	Catalyst particles radius (m)
k_{ss}	Conductive heat transfer coefficient of stainless steel (W m^{-1}K^{-1})
$\overline{D_{ij}}$	Diffusion coefficient (m^2 s^{-1})
$\underline{U}$	Velocity field
k	Permeability of the catalyst bed
ω_i	Mass fraction of the ith gas species
x_j	Molar fraction of components
k_{eff}	Effective coefficient of conductive heat transfer of the catalytic bed
θ_H	Fraction of membrane surface covered by H atoms
ε_{bed}	Porosity of catalyst bed
τ	Tortuosity
P_M	Permeability coefficient

Abbreviations

MD	Methanol Decomposition
MSR	Methanol Steam Reforming
WGS	Water Gas Shift

Subscripts

Tube	In the tube side of reactor
Shell	In the shell side of reactor
Conv	Convection transformation
Cond	Conduction transformation
Bed	Catalytic bed
eff	Effectiveness parameter
perm	permeate side value

Greek symbols

δ	Membrane thickness (m)
ρ_B	bulk density of reforming catalyst (kg m^{-3})

References

[1] Andrews, J., Shabani, B., 2012, Re-envisioning the role of hydrogen in a sustainable energy economy, International journal of hydrogen energy, 37(2), 1184-1203. https://doi.org/10.1016/j.ijhydene.2011.09.137

[2] Cacciola, G., Antonucci, V., Freni, S., 2001, Technology up date and new strategies on fuel cells, Journal of power sources, 100(1-2), 67-79. https://doi.org/10.1016/S0378-7753(01)00884-9

[3] King, J.M., O'Day, M.J., 2000, Applying fuel cell experience to sustainable power products. Journal of Power Sources, 86(1-2), 16-22. https://doi.org/10.1016/S0378-7753(99)00443-7

[4] Ramirez, D., Beites, L.F., Blazquez, F., Ballesteros, J.C., 2008, Distributed generation system with PEM fuel cell for electrical power quality improvement, International Journal of Hydrogen Energy, 33(16), 4433-4443. https://doi.org/10.1016/j.ijhydene.2008.06.002

[5] Iulianelli, A., Ribeirinha, P., Mendes, A., Basile, A, 2014, Methanol steam reforming for hydrogen generation via conventional and membrane reactors: a review. Renewable and Sustainable Energy Reviews, 29, 355-368. https://doi.org/10.1016/j.rser.2013.08.032

[6] Basile, A., Parmaliana A., Tosti, S., Iulianelli, A., Gallucci, F., Espro, C., Spooren, J., 2008, Hydrogen production by methanol steam reforming carried out in membrane reactor on Cu/Zn/Mg-based catalyst, Catalysis Today, 137(1), 17-22. https://doi.org/10.1016/j.cattod.2008.03.015

[7] Chen, Y., Wan, Y., Xu, H., Xiong, G., 2008, Hydrogen production capacity of membrane reformer for methane steam reforming near practical working conditions, Journal of Membrane Science, 322(2), 453-459. https://doi.org/10.1016/j.memsci.2008.05.051

[8] Olah, G.A., 2005, Beyond oil and gas: The methanol economy. Angewandte Chemie International Edition, 44(18), 2636-2639. https://doi.org/10.1002/anie.200462121

[9] Telotte, J.C., Kern, J., Palanki, S., 2008, Miniaturized methanol reformer for fuel cell powered mobile applications, International Journal of Chemical Reactor Engineering, 6(1). https://doi.org/10.2202/1542-6580.1731

[10] Zhang, X., Hu, H., Zhu, Y., Zhu, S., 2006, Methanol steam reforming to hydrogen in a carbon membrane reactor system, Industrial & engineering chemistry research, 45(24), 7997-8001. https://doi.org/10.1021/ie060414m

[11] Talaghat, M.R., Naamaki, N., 2021, Mathematical modeling of hydrogen production using methanol steam reforming in the coupled membrane reactor when the output materials of the reformer section is used as feed for the combustion section, International Journal of Hydrogen Energy, 46(2), 2282-2295. https://doi.org/10.1016/j.ijhydene.2020.10.128

[12] Frank, B., Jentoft, F.C. Soerijanto, H., Kröhnert, J., Schlögl, R., Schomäcker, R., 2007, Steam reforming of methanol over copper-containing catalysts: Influence of support material on microkinetics, Journal of Catalysis, 246(1), 177-192. https://doi.org/10.1016/j.jcat.2006.11.031

[13] Purnama, H., Ressler, T., Jentoft, R.E., Soerijanto, H., Schlögl, R., Schomäcker, R., 2004, CO formation/selectivity for steam reforming of methanol with a commercial CuO/ZnO/Al2O3 catalyst, Applied Catalysis A: General, 259(1), 83-94. https://doi.org/10.1016/j.apcata.2003.09.013

[14] Lattner, J.R., Harold, M.P., 2005, Comparison of methanol-based fuel processors for PEM fuel cell systems, Applied Catalysis B: Environmental, 56(1-2), 149-169. https://doi.org/10.1016/j.apcatb.2004.06.024

[15] Ghasemzadeh, K., Morrone, P., Liguori, S., Babaluo, A.A., Basile, A, 2013, Evaluation of silica membrane reactor performance for hydrogen production via methanol steam reforming: modeling study, International journal of hydrogen energy, 38(36), 16698-16709. https://doi.org/10.1016/j.ijhydene.2013.06.121
[16] Peppley, B.A., Amphlett, J.C., Kearns, L.M., Mann, R.F., 1999, Methanol–steam reforming on Cu/ZnO/Al2O3 catalysts, Part 2. A comprehensive kinetic model, Applied Catalysis A: General, 179(1-2), 31-49. https://doi.org/10.1016/S0926-860X(98)00299-3
[17] Zhang, L., Pan, L., Ni, C., Sun, T., Zhao, S., Wang, S., Wang, A., Hu, Y., 2013, CeO2–ZrO2-promoted CuO/ZnO catalyst for methanol steam reforming, International Journal of Hydrogen Energy, 38(11), 4397-4406. https://doi.org/10.1016/j.ijhydene.2013.01.053
[18] Chaubey, R., Sahu, S., James, O.O., Maity, S., 2013, A review on development of industrial processes and emerging techniques for production of hydrogen from renewable and sustainable sources, Renewable and Sustainable Energy Reviews, 23, 443-462. https://doi.org/10.1016/j.rser.2013.02.019
[19] Rohde, M.P., Schaub, G., Khajavi, S., Jansen, J.C., Kapteijn, F., 2008, Fischer–Tropsch synthesis with in situ H_2O removal–Directions of membrane development, Microporous and Mesoporous Materials, 115(1-2), 123-136. https://doi.org/10.1016/j.micromeso.2007.10.052
[20] Hara, S., Xu, W.-C., Sakaki, K., Itoh, N., 1999, Kinetics and hydrogen removal effect for methanol decomposition, Industrial & engineering chemistry research, 38(2), 488-492. https://doi.org/10.1021/ie980456d
[21] Barbieri, G., Di Maio, F.P., 1997, Simulation of the Methane Steam Re-forming Process in a Catalytic Pd-Membrane Reactor, Industrial & Engineering Chemistry Research, 36(6), 2121-2127. https://doi.org/10.1021/ie9601615
[22] Palo, D.R., Dagle, R.A., Holladay, J.D., 2007, Methanol steam reforming for hydrogen production, Chemical reviews, 107(10), 3992-4021. https://doi.org/10.1021/cr050198b
[23] Faungnawakij, K., Kikuchi, R., Eguchi, K., 2006, Thermodynamic evaluation of methanol steam reforming for hydrogen production, Journal of Power Sources, 161(1), 87-94. https://doi.org/10.1016/j.jpowsour.2006.04.091
[24] Pasel, J., Emonts, B., Peters, R., Stolten, D., 2001, A structured test reactor for the evaporation of methanol on the basis of a catalytic combustion, Catalysis today, 69(1-4), 193-200. https://doi.org/10.1016/S0920-5861(01)00369-8
[25] Chu, X., Zeng, X., Zheng, T., Zhuang, W., Yang, Y., Zhou, W., Hong, Y., 2020, Structural design and performance research of methanol steam reforming microchannel for hydrogen production based on mixing effect, International journal of hydrogen energy, 45(41), 20859-20874. https://doi.org/10.1016/j.ijhydene.2020.05.190
[26] Israni, S.H., Harold, M.P., 2011, Methanol steam reforming in single-fiber packed bed Pd–Ag membrane reactor: Experiments and modeling, Journal of Membrane Science, 369(1-2), 375-387. https://doi.org/10.1016/j.memsci.2010.12.029
[27] Parvazinia, M., Nassehi, V., Wakeman, R. J., Ghoreishy, M. H. R., 2006, Finite element modelling of flow through a porous medium between two parallel plates using the Brinkman equation, Transport in Porous Media, 63(1), 71-90. https://doi.org/10.1007/s11242-005-2721-2
[28] Curtiss, C.F., Bird, R.B., 1999, Multicomponent diffusion, Industrial & Engineering Chemistry Research, 38(7), 2515-2522. https://doi.org/10.1021/ie9901123
[29] Gunn, D.J., 1987, Axial and radial dispersion in fixed beds, Chemical Engineering Science, 42(2), 363-373. https://doi.org/10.1016/0009-2509(87)85066-2
[30] Specchia, V., Baldi, G., Sicardi, S., 1980, Heat transfer in packed bed reactors with one phase flow, Chemical Engineering Communications, 4(1-3), 361-380. https://doi.org/10.1080/00986448008935916
[31] Qureshi, F., Ahmad, F., Idrees, M., Asif Khan, A., Zaidi, S., 2021, Simulation of methanol steam reforming process for the production of hydrogen, Indian Chemical Engineer, 63(1), 99-116. https://doi.org/10.1080/00194506.2019.1689186